Int J Adv Manuf Technol (2016) 84:2113–2126
DOI 10.1007/s00170-015-7864-x

ORIGINAL ARTICLE

Improvement of useful flow rate of grinding fluid with simulation schemes

Yanbin Zhang[1] · Changhe Li[1] · Qiang Zhang[1] · Dongzhou Jia[1] · Sheng Wang[1] · Dongkun Zhang[1] · Cong Mao[2]

Received: 5 May 2015 / Accepted: 13 September 2015 / Published online: 24 September 2015

Abstract In previous studies, the improvement of the useful flow and flow rate of grinding fluid has been investigated via modeling, simulation, and experiment. Optimized grinding parameters have been achieved. A detailed assessment of the improvement in the useful flow rate of grinding fluid, which optimizes the grinding fluid supply, has been published in the *International Journal of Advanced Manufacturing Technology* (Li et al. Int J Adv Manuf Technol 75:1587–1604, 2014). Then, a detailed experimental study on the improvement in the useful flow rate of grinding fluid has been published in the *International Journal of Advanced Manufacturing Technology* (Li et al. Int J Adv Manuf Technol 1–10. doi:10.1007/s00170-015-7230-z, 2015), in which the influence of grinding wheel speed, grinding fluid jet velocity, particle size, and bulk porosity on useful flow and useful flow rate was analyzed. In this paper, a new method of *air scraper* is presented and simulated with focus on the air boundary layer and reflux around the grinding wheel. In view of the influence of the gas barrier of grinding wheels on the effective supply of grinding fluid, the effect of the scraper on the gas barrier layer was analyzed through the grinding flow field simulation under unified grinding parameters. Using the *air scraper* to destroy the gas barrier layer is proposed, and a supply scheme is designed to improve the useful flow rate. Results show that using the scraper has a certain effect on the weakening of the grinding gas barrier layer. In the grinding process, using the scraper can reduce the obstacles to grinding fluid supply, thereby improving the useful flow of grinding fluid into grinding wheel workpieces. The distance between the front end of the plane scraper and the grinding wheel is 10 μm, with a large circular boot-shaped nozzle. Alternatively, the distance between the front end of the nozzle and the grinding wheel surface is 50 μm, which can increase the useful rate of flow of grinding fluid.

Keywords Scraper · Airbond layer · Grinding fluid · Useful flow rate · Useful flow · Fluid supply

1 Introduction

In the grinding process, a large amount of energy is consumed to remove the material per unit of volume [1]. The energy is then transformed into heat concentrated on the grinding zone. Heat accumulation causes a high-temperature condition, leading to thermal injury, such as burns, cracks, and metallurgical changes, of the workpiece [2]. This condition also leads to workpiece deformation and other consequences [3]. Using liquid has been considered to reduce the temperature in the grinding zone. In this regard, flood cooling technique is applied in the grinding. Given that the grinding fluid has lubricating, cooling, and washing functions, this fluid can be casted in the grinding zone to reduce the temperature. In the process, the grinding fluid also removes debris. Compared with abrasive grinding, flood grinding can improve the surface quality of the workpiece [4, 5]. The grinding fluid cools the workpiece through heat convection, which reduces the grinding temperature of the workpiece. For flood cooling, a mass flow of the grinding fluid is used to cast the wedge-shaped area between the grinding wheel and the workpiece [6]. A large

✉ Changhe Li
sy_lichanghe@163.com

[1] School of Mechanical Engineering, Qingdao University of Technology, 266033 Qingdao, China

[2] College of Automotive and Mechanical Engineering, Changsha University of Science and Technology, 410114 Changsha, China

amount of grinding fluid cannot easily enter the interface of the grinding wheel and workpiece because of the airbond formed from the high-speed revolution of the grinding wheel and other factors [7–9]. Grinding fluid, which actually goes through the wheel/workpieces, is called useful flow. The ratio of the useful flow and the nozzle flow is called useful flow rate. In fact, the useful flow rate that enters the interface is only 5–40 % [10]. Only the useful flow can lubricate the grinding action, prevent wheel wear and clogging, maintain low surface roughness, and prevent excessive grinding temperatures. Thus, a large amount of grinding fluid leaks out during grinding. Wasted grinding fluid should be recycled and processed because of the low effective utilization rate of this fluid [11]. The expenses on purchasing and processing the grinding fluid account for a high proportion of the total cost of machining. Liquid waste disposal is also costly, accounting for up to 54 % of the total cost of the grinding fluid [12]. In the process of disposal, grinding fluid may be volatilized, leaked, or spilled in vaporific form, thereby causing environmental deterioration of working places, land and water contamination, and ecological destruction [13]. Volatilized grinding fluid under heat is harmful to the health of operators if it directly contacts human body, thereby triggering a range of skin, respiratory tract, and lung diseases [14].

Many researchers have explored the field of grinding fluid flow and useful flow rate to achieve the optimum output of the grinding fluid and to minimize the total cost required in grinding.

Kaliszer and Trmal [15] examined the effects of the airbond layer of the grinding wheel on the useful grinding fluid flow. When the nozzle jet velocity is greater than the critical velocity, the grinding fluid punctures the airbond layer and passes through the grinding zone by the drag force of the grinding wheel. The critical velocity is derived theoretically under the premise that grinding fluid momentum is equal to the momentum of the boundary air layer. The airbond layer is formed by destroying the high-speed airflow around the wheel using an air scraper. The researchers also conducted an experiment to verify the accuracy of their theoretical analysis.

Campbell [16, 17] measured and analyzed the pressure in the contact zone and proposed the optimal grinding fluid supply conditions. They also compared the useful grinding fluid flow passing through the grinding zone in instances when the air scraper is used and not used. The study showed that using the air scraper increases the useful flow rate of the grinding fluid.

Ganesan and Guo [18, 19] measured the hydrodynamic pressure in the wedge-shaped grinding wheel/workpiece contact zone. The results showed that hydrodynamic pressure increases with the increase of grinding wheel velocity. Cutting depth and feed speed had minimal influence on hydrodynamic pressure. The smaller the particle size of the grinding wheel is, the greater the hydrodynamic pressure is. The largest hydrodynamic pressure was produced at the convergence entrance of the grinding zone. The study also established a theoretical model of the contact zone and hydrodynamic force based on classic hydrodynamics and laminar theory. Chang et al. [20] considered the effect of wheel porosity. According to the law of conservation, the study built a mathematical model of dynamic pressure of grinding fluid during intermittent-creep feed grinding. The simulation results showed that a large supply of grinding fluid produces substantial hydrodynamic pressure.

Klocke et al. [21] simulated the hydrodynamic pressure from the high-speed grinding fluid. They also assumed the hydrodynamic effect in the grinding zone as *laminar flow*, and the wheel and the workpiece surfaces were smooth. The moving speed of the workpiece was considerably smaller than the peripheral velocity of the grinding wheel; thus, the moving speed can be ignored. The grinding fluid did not slide on the wheel surface. In other words, the velocity of the fluid attached to the wheel was equal to the velocity of the grinding wheel. Along the thickness direction of the grinding fluid, the pressure changes can be ignored. Compared with that of the viscous force, the effect of inertial force can be ignored. Reynolds equation was used to calculate the hydrodynamic pressure at the convergence gap of the grinding wheel and the workpiece.

Hryniewicz et al. [22] employed the lubrication theory to study the rules of hydrodynamic pressure distribution in the grinding zone under two conditions. One was a smooth wheel and the other was the surface roughness of the grinding wheel. They [23] also applied the Reynolds equation to establish a two-dimensional mathematical model, which was verified with experiments. In addition, the researchers presented the quantitative relationship among the fluid dynamic pressure, velocity of grinding wheel, and minimum clearance between the grinding wheel and the workpiece.

Considering the wheel porosity effect, Guo and Malkin [24] applied mass conservation equation and momentum conservation equation to establish the mathematical model of useful flow rate in the grinding zone. The model can forecast tangential velocity, radial velocity, permeation depth in the grinding wheel, and useful flow of the grinding fluid. The study demonstrated that the nozzle position, grinding fluid jet velocity, and wheel porosity are the three main factors that influence the useful flow.

Engineer et al. [25] designed an experimental device to measure the grinding fluid flow (i.e., the useful flow) in the grinding zone. The study determined the proportional relationship between the useful grinding fluid flow and the nozzle flow. The study also proved that the useful flow rate mainly depends on the grinding wheel porosity and nozzle position. The finishing of the grinding wheel played a secondary role in the process. This observation was mainly attributed to the effect of the finishing of the grinding wheel on its surface

porosity. Meanwhile, the workpiece velocity and cutting depth of the wheel slightly influenced the useful flow.

Gviniashvili et al. [26, 27] proposed a model of the useful flow rate and stated that the useful flow rate passing through the contact zone can be used in the function of the main shaft power of fluid acceleration, velocity of grinding wheel, and fluid jet velocity. They also verified their model through experiments. They [28, 29] studied the hydrodynamic pressure and the flow of grinding wheel/workpiece contact zone. They derived the mathematical model with the energy conservation equation for the useful grinding fluid flow. They determined that the useful flow is the function of hydrodynamic pressure within the grinding zone, nozzle flow, fluid density, and velocity of grinding wheel. Relevant experiments were also conducted to explore the variation rules of the useful grinding fluid flow as influenced by various elements.

Morgan et al. [10] analyzed the grinding fluid flow and supply modes of the grinding fluid required by the grinding process. The results showed that the useful grinding fluid flow accounts for one-fourth of the supply. Thus, a large amount of grinding fluid was wasted. The improved system enabled the actual useful grinding fluid flow to reach a level close to the theoretical useful flow. The theoretical useful flow was dependent on wheel porosity and grinding wheel velocity. However, the actual useful grinding fluid flow was dependent on the nozzle position, nozzle shape, grinding fluid jet flow, and jet velocity. Li et al. [30–35] analyzed the flow field velocity and pressure distribution rules in the grinding zone during grinding. They established a corresponding mathematical model and conducted a verification experiment. Zheng et al. [36] studied the variation rules of the grinding fluid dynamic pressure in wedge-shaped space. They applied gas–liquid two-phase flow theory in the theoretical research on grinding flow field dynamic pressure. The simulation results of the theoretical model were identical to those of the actual experimental results.

The grinding fluid plays a key role in grinding throughout the development of grinding technology. Many researchers around the world [37–47] have conducted exploratory studies on the flow rules of the grinding fluid. Mandal et al. [45–47] developed a pneumatic barrier and compound nozzle setup to control the stiff air layer around the grinding wheel, and a remarkable amount of reduction in pressure of the air layer was observed at the fluid flow zone. In the grinding process, reduction of the grinding forces and surface roughness was observed in the pneumatic barrier setup.

Compared with studies on other key grinding technologies, studies on the flow field of the grinding zone are limited. Certain phenomena were observed through the study. However, causes behind these phenomena were not elaborated. Studies on the flow field of grinding zone were flawed. In actual application, the grinding fluid was mainly fed by pouring. A German survey [48] of automobile manufacturers showed that tools account for only 2–4 % of the processing costs. However, those related with grinding fluid account for 7–17 % of the costs, which is 3–5 times higher than the processing cost of the tools. Grinding characteristics cause a very high level of difficulty for dry grinding without grinding fluid. Thus, a study, which meets the cooling and lubrication needs, reduces the grinding fluid consumption, improves the useful flow rate of the grinding fluid, optimizes grinding fluid supply, and presents highly important theoretical and practical implications.

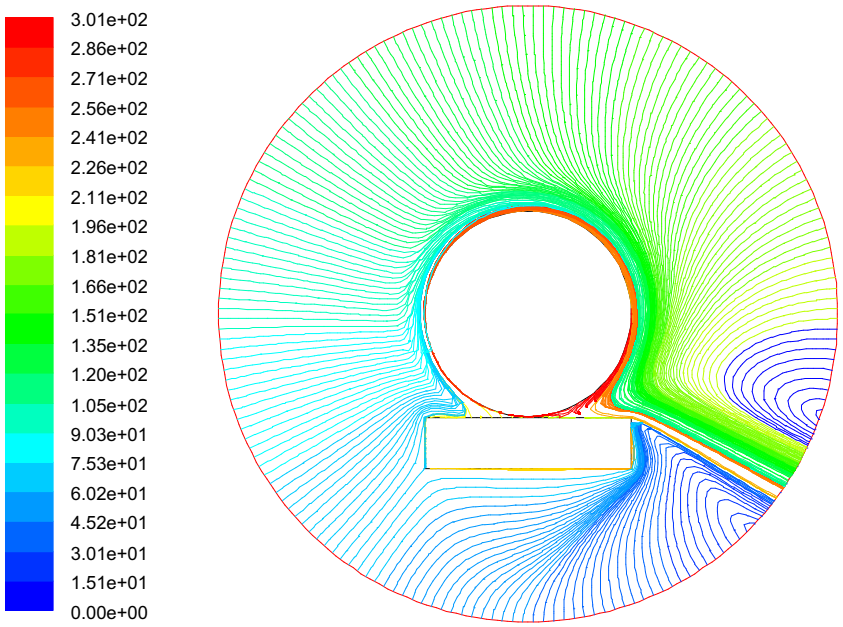

Fig. 1 Motion pattern of the airflow field

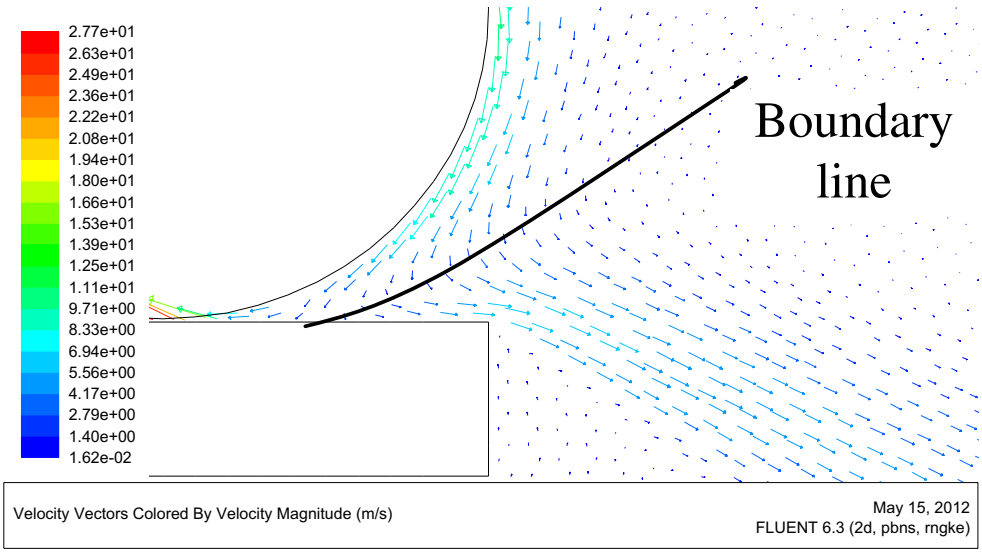

Fig. 2 Velocity vector figure in the wedge-shaped zone

2 Scheme to improve useful flow rate of grinding fluid

Figures 1 and 2 illustrate an obvious airbond layer on the wheel surface of the airflow field in the plane grinding. In addition, the airflow velocity in the wedge-shaped zone between the wheel and the workpiece presented certain patterns because of the existence of the workpiece. Reflux also occurred in the inflow. Meanwhile, pressure in the inflow was considerably large while negative pressure occurred in the outflow zone, which was close to the minimum clearance.

Reflux occurred in front of the inflow, thereby indicating that the reverse flow appears on the workpiece surface near the grinding zone. Figure 2 shows the partially magnified velocity vector figure in the wedge-shaped zone. The arrow direction represents the direction of the velocity. Above the boundary line, airflow direction was the same as the peripheral velocity of the rotating wheel. The horizontal velocity pointed at the outflow from the inflow zone, which was conducive to the injection of the grinding fluid in the wedge-shaped clearance. However, the airflow direction under the boundary line was reverse to the peripheral velocity of the rotating wheel. The horizontal velocity pointed at the inflow from the outflow zone, which was not conducive to the injection of the grinding fluid in the wedge-shaped clearance. When the nozzle sprayed the grinding fluid into the wedge-shaped zone, the spraying direction should be kept above the boundary line if possible, which was conducive to the injection of the grinding fluid in the wedge-shaped clearance. Related studies showed that when the nozzle axis formed a certain angle (15°–20°) with the workpiece surface, the grinding fluid tends to enter the wedge-shaped clearance easily.

Grinding fluid, which actually goes through the wheel/workpieces, is called useful flow. The ratio of the useful flow and nozzle flow is called the useful flow rate. Only the useful flow can fully provide lubrication to grinding activities. Thus, wheel wearing and clogging are prevented, low surface roughness is maintained, and generation of high grinding temperature is prevented. Some other flows, which pass by the cutting zone, can only provide partial support to remove heat from the workpiece and the grinding wheel. The improved grinding liquid flow rate mentioned in this paper is achieved with the change of the location and shape of the scraper under the condition of the constant grinding parameters (including the peripheral speed of the grinding wheel and the jet speed of the grinding fluid).

The preceding analysis indicated that the returned flow in the gas barrier layer and grinding fluid entrance block the effective supply of grinding fluid. Therefore, the ranges in

Table 1 Optimization goal and procedures

Project	Details
Optimization goal	The air scraper is used to damage the gas barrier layer of the wheel rotation and to improve the flow rate of the grinding fluid.
Optimization procedures	(1) The effect of the scraper on the gas barrier layer is analyzed through the simulation of the grinding gas flow field.
	(2) The scheme of the scraper is designed to improve the flow rate of the grinding fluid.
	(3) The scraper shape and location are optimized to improve the flow rate of the grinding fluid through the simulation research on gas–liquid two-phase flow.
	(4) The optimization scheme is achieved through simulation research and theoretical analysis.

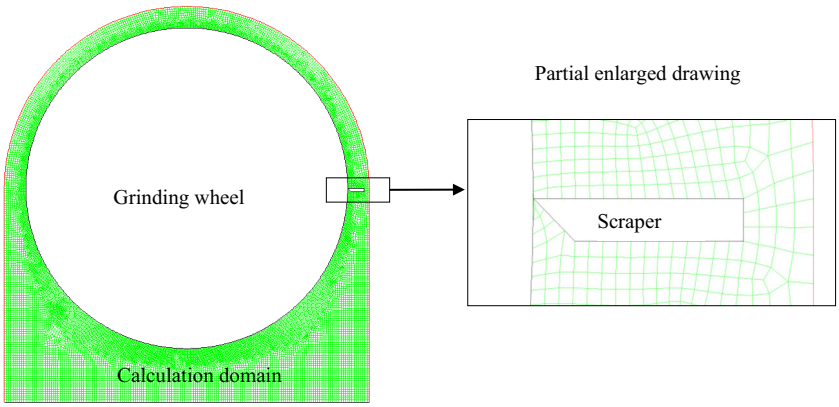

Fig. 3 Geometric model for simulation

which the solutions are searched for are determined. First, in this paper, the measures to raise the flow rate of the grinding fluid are presented in view of the aforementioned two aspects. Second, the air scraper must be used to damage the gas barrier layer of the wheel rotation and to improve the flow rate of the grinding fluid. Third, the optimization parameters include scraper shape, scraper location, and distance between the scraper and the nozzle. According to the research ranges, the goal and the procedures of optimization are shown in Table 1.

3 Simulation of airflow field with scraper

3.1 Simulation model

Based on simulation and analysis of the airflow field after using the scraper, the influence of scraper on the gas barrier layer grinding wheel rotation was explored. The simulation model is shown in Fig. 3.

Simulation was conducted under the unified grinding parameters mentioned in this paper. The grinding parameters are shown in Table 2. The boundary condition between the grinding wheel and the workpiece was the wall boundary. The boundary condition of the nozzle outlet was the velocity inlet. The boundary condition near the nozzle was the wall boundary, and the peripheral boundary condition of the calculation domain was the pressure outlet.

The included angle between the nozzle axis and the workpiece surface was taken as 15° to avoid the hindering effects of reflow at the inlet of the grinding zone on feeding grinding fluid. In this way, the grinding fluid could enter the grinding contact zone between the grinding wheel and the workpiece smoothly, and the cooling and lubricating functions could be sufficiently performed.

3.2 Simulation parameters

.msh files output by Gambit were introduced in Fluent, and a series of simulation parameters were set. Table 3 shows the setting of the Fluent simulation parameters.

In simulation parameter settings, unsteady pressure-based solver was used. This solver needed a volume of fluid (VOF) multiphase model for the simulation of gas–water two-phase flow in the grinding flow field. k–ε viscous model was chosen as the viscous model. The materials in the computational domain were air and water, in which water was chosen as the grinding fluid (density was 998.2 kg/m^3 and dynamic viscosity was 0.001003 Pa·s). Phase settings were necessary in simulation. In this case, air and water (grinding fluid) were set as primary phase and secondary phase, respectively, and the operating pressure was 101,325 Pa, in which the pressure value in the simulation result was relative pressure. Considering the influence of fluid gravity, we set y-direction acceleration of

Table 2 Grinding parameters

Parameter	Size
Diameter of grinding wheel	300 mm
Size of scraper	(15×3) mm
Size of workpiece	(200×50) mm
Minimum clearance between grinding wheel and workpiece	49 μm
Semicircle diameter of computational domain outer boundary	340 mm
Nozzle gap	2 mm
Included angle between nozzle axis and workpiece surface	15°
Radial distance from nozzle to wheel surface	10 mm

Table 3 Setting of simulation parameters

Simulation parameter	Setting
Solver	2D single-precision solver; pressure based; unsteady
Multiphase model	Volume of fluid (VOF); number of phases: 2
Viscous model	*k*–epsilon; standard; standard wall functions
Fluent fluid materials	Air; water–liquid
Phases	Primary phase: air; secondary phase: water
Operating pressure	101,325 Pa; *y*-direction acceleration of gravity −9.81
Boundary conditions	Boundary pressure of pressure outlet was 0; circular velocity of grinding wheel was 30 m/s; wall boundary of workpiece was static

gravity as −9.81 m/s^2. The boundary condition setting is listed in Table 3.

Nozzle velocities were 5, 10, 20, and 30 m/s, and they should still set the related parameters of turbulence. The calculation of turbulence-related parameters was based on Eqs. (1) to (6). Volume fraction value was set as 1 in the secondary phase velocity inlet boundary option *multiphase*. Thus, the fluid squirting from the velocity inlet was water. *Backflow volume fraction* value was set as 0 in the secondary phase pressure outlet boundary option *multiphase*. The grinding wheel was set as the clockwise rotation model, and the workpiece was static. The rotation speeds of the grinding wheel dynamic boundary were −200, −266.67, −333.33, −400, −533.33, −666.67, and −800 rad/s. The circular velocities of the grinding wheel were 30, 40, 50, 60, 80, 100, and 120 m/s, respectively.

The calculation of turbulence-related parameters in the simulation is presented subsequently in this paper.

For tubes with noncircular sections, R_e can be calculated with the following equation:

$$R_e = \frac{4vR_H}{\upsilon}, \tag{1}$$

where R_H is the hydraulic radius of passage section, which was equivalent to the proportion between the useful sectional area of fluid A and its wetted perimeter (perimeter between liquid and solid wall) χ; v is the flow velocity of the grinding fluid; and υ is the kinematic viscosity of the grinding fluid.

The hydraulic radius of tubes with a circular section and a diameter of d is $R_H = A/\chi = \frac{1}{4}\pi d^2/(\pi d) = d/4$.

When the grinding fluid was jetted at the minimum valuing velocity (i.e., 5 m/s), the value could be substituted in the following equation:

$$R_e = \frac{4vR_H}{\upsilon} = \frac{4 \times 5 \times \left(2 \times 10^{-3} \times 1/2.004\right) \times 998.2}{0.001} = 19924.2.$$

Given that R_e>2300, the grinding fluid was turbulent flow. The Reynolds number was positively proportional to the flow velocity of the grinding fluid. The Reynolds number increased accordingly when the grinding fluid jet velocity increased. Thus, all of the four grinding fluid jet velocities selected in our simulation had turbulent flow. The *k*–ε turbulence model was selected among the simulation parameters.

The computational formula of turbulence intensity I is

$$I = 0.16R_e^{-\frac{1}{8}}. \tag{2}$$

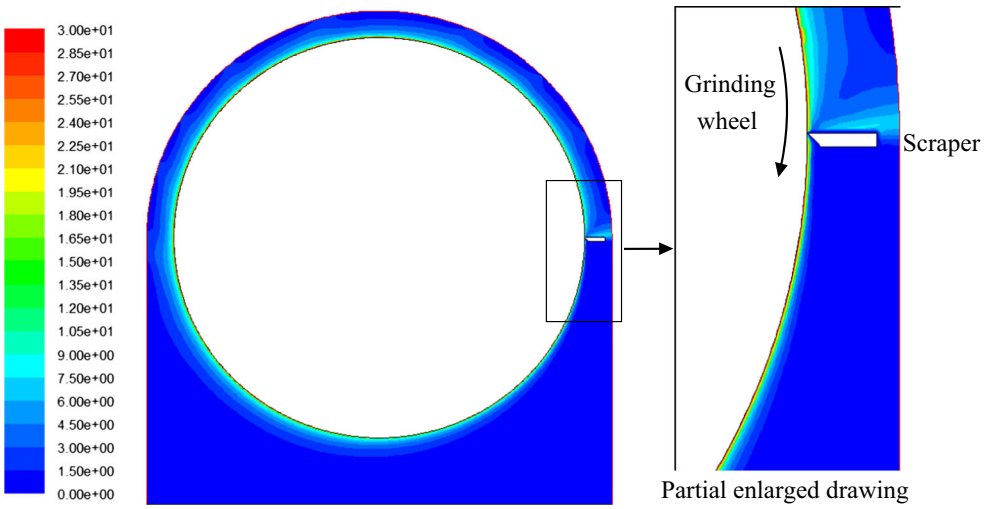

Fig. 4 Velocity distribution of airflow field in grinding

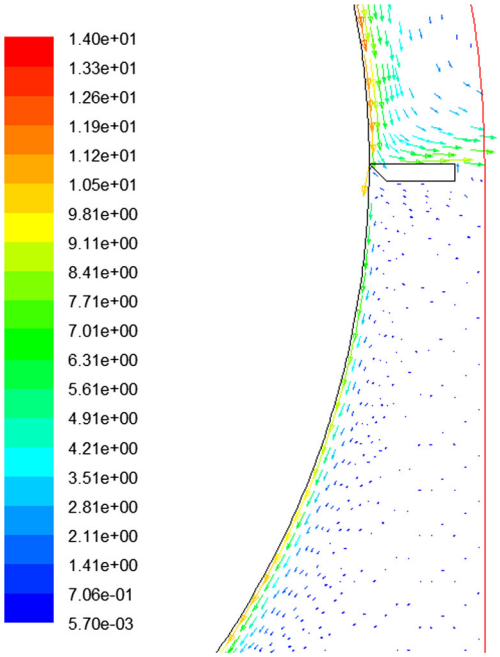

Fig. 5 Velocity vector distribution of airflow field near the scraper

The computational formula of turbulent kinetic energy k is

$$k = \frac{3}{2}(UI)^2, \tag{3}$$

where U is the flow velocity of the grinding fluid.

The computational formula of characteristic dimension (hydraulic diameter) L is

$$L = d_{\mathrm{H}} = 4R_{\mathrm{H}} = \frac{4A}{\chi} = \frac{4 \times 1 \times 2 \times 10^{-3}}{2.004} = 3.992\,mm. \tag{4}$$

The computational formula of turbulent length scale l is

$$l = 0.07L \tag{5}$$

The computational formula of turbulent dissipation rate ε is

$$\varepsilon = c_{\mu}^{0.75}\frac{k^{1.5}}{l}. \tag{6}$$

3.3 Governing equation of simulation solution

After the parameter setting, the governing equation list of solution controls listed all governing equations to be solved, namely flow, volume fraction, and turbulence. The flow equation included the equation of continuity and momentum conservation equation. Volume fraction was an equation for volume fraction. Turbulence indicated k–ε turbulence model. The specific governing equations are as follows:

(1) Equation of continuity

$$\frac{\partial \rho}{\partial t} + \nabla\cdot\left(\rho\vec{v}\right) = 0, \tag{7}$$

where ρ is fluid density, kg/m^3; $\vec{v}$ is fluid velocity vector, m/s; and t is time, s.

(2) Momentum conservation equation

$$\frac{\partial\left(\rho\vec{v}\right)}{\partial t} + \nabla\cdot\left(\rho\vec{v}\vec{v}\right) = -\nabla\rho + \nabla\cdot\left[\mu\left(\nabla\vec{v} + \nabla\vec{v}^{T}\right)\right] + \rho\vec{g} + \vec{F}, \tag{8}$$

where μ is fluid dynamic viscosity, Pa·s; $\vec{g}$ is acceleration of gravity, m/s^2; and $\vec{F}$ is applied body force, N.

(3) Physical attribute equation

$$\rho = \alpha_{\mathrm{L}}\rho_{\mathrm{L}} + \alpha_{\mathrm{G}}\rho_{\mathrm{G}}, \tag{9}$$

$$\mu = \alpha_{\mathrm{L}}\mu_{\mathrm{L}} + \alpha_{\mathrm{G}}\mu_{\mathrm{G}}, \tag{10}$$

where α_{L} and α_{G} are liquid phase and gas phase volume fraction, respectively; ρ_{L} and ρ_{G} are liquid phase and gas

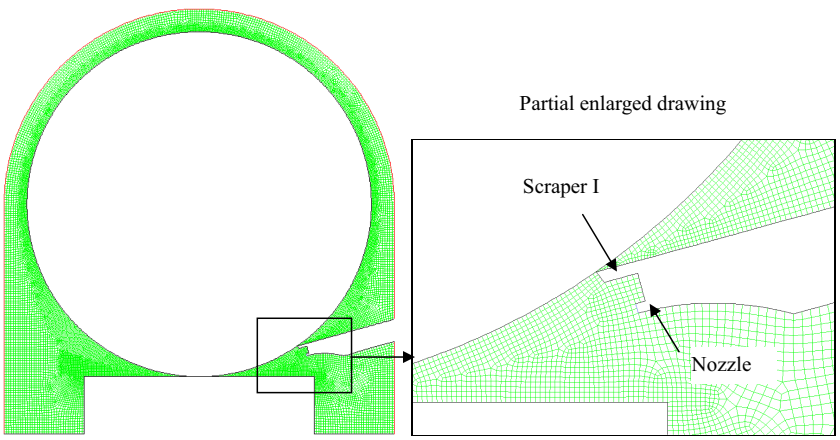

Fig. 6 Scraper I model

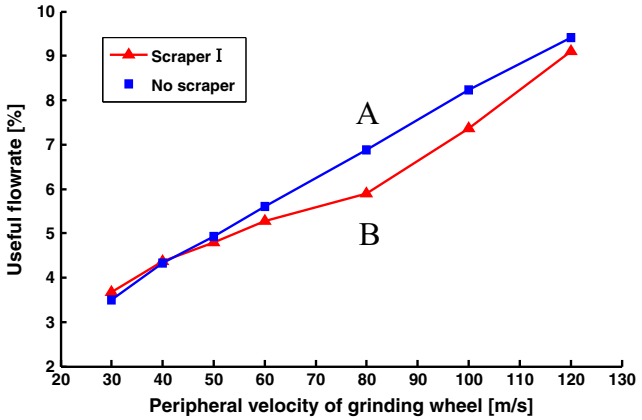

Fig. 7 Comparison of useful flow rate in the conditions with and without scraper I (v_j=20 m/s)

phase density, respectively, kg/m^3; and μ_L and μ_G are liquid phase and gas phase dynamic viscosity, respectively, Pa·s.

(4) Volume fraction equation

$$\frac{\partial \alpha_G}{\partial t} + \vec{v} \cdot \nabla \alpha_G = 0 \tag{11}$$

(5) k–ε turbulence model

A standard k–ε model is the main tool in engineering flow field calculation. It is a semirational formula and is concluded from experiments. Thus, it presents features such as wide application range, economic usage, and reasonable precision. The basic transport equation is

$$\frac{\partial}{\partial t}(\rho k) + \frac{\partial}{\partial X_i}(\rho k u_i) = \frac{\partial}{\partial X_j}\left[\left(\mu + \frac{\mu_t}{\sigma_k}\right)\frac{\partial k}{\partial X_j}\right] + G_k - \rho\varepsilon - Y_M, \tag{12}$$

$$\frac{\partial}{\partial t}(\rho \varepsilon) + \frac{\partial}{\partial X_i}(\rho \varepsilon u_i) = \frac{\partial}{\partial X_j}\left[\left(\mu + \frac{\mu_t}{\sigma_\varepsilon}\right)\frac{\partial \varepsilon}{\partial X_j}\right] + C_{1\varepsilon}\frac{\varepsilon}{k}G_k - C_{2\varepsilon}\rho\frac{\varepsilon^2}{k}, \tag{13}$$

where k is turbulence energy; ε is turbulent dissipation rate; μ_t is turbulent viscosity; G_k is the generation term of turbulence energy caused by average velocity gradient; Y_M represents the contribution of fluctuation expansion in compressible turbulent flow; $C_{1\varepsilon}$ and $C_{2\varepsilon}$ are empirical constants; and σ_k and σ_ε are Prandtl numbers corresponding to the turbulence energy k and turbulent dissipation rate ε, respectively.

Turbulent viscosity μ_t can be determined with the following equation:

$$\mu_t = \rho C_\mu \frac{k^2}{\varepsilon}, \tag{14}$$

where C_μ is a constant; the model constants are $C_{1\varepsilon}$=1.44, $C_{2\varepsilon}$=1.92, C_μ=0.09, σ_k=1, and σ_ε=1.3.

4 Analysis of simulation results

Figure 4 illustrates the air velocity distribution near the rotating grinding wheel and around the scraper. Around the rotating wheel, the presence of the gas barrier layer is obvious, which hinders the grinding fluid supply. We can observe the influence of the scraper on the gas barrier layer combined with partial enlargement of the scraper. The wheel rotates clockwise. Given the existence of the scraper, a gas barrier layer is thick at the top, and the air velocity in the gas barrier layer is large. The scraper also forms a gas barrier layer with a certain thickness. The gas barrier layer gradually thickens with increasing distance from the scraper.

Figure 5 shows the flow field velocity vector near the scraper. This figure illustrates that the air velocity distribution is near the scraper, and the arrow indicates the speed direction. Above the scraper, the gas barrier layer is thick and the speed is quick. The air flows out along the blade horizontally from the outlet boundary. By contrast, the gas barrier layer is thin

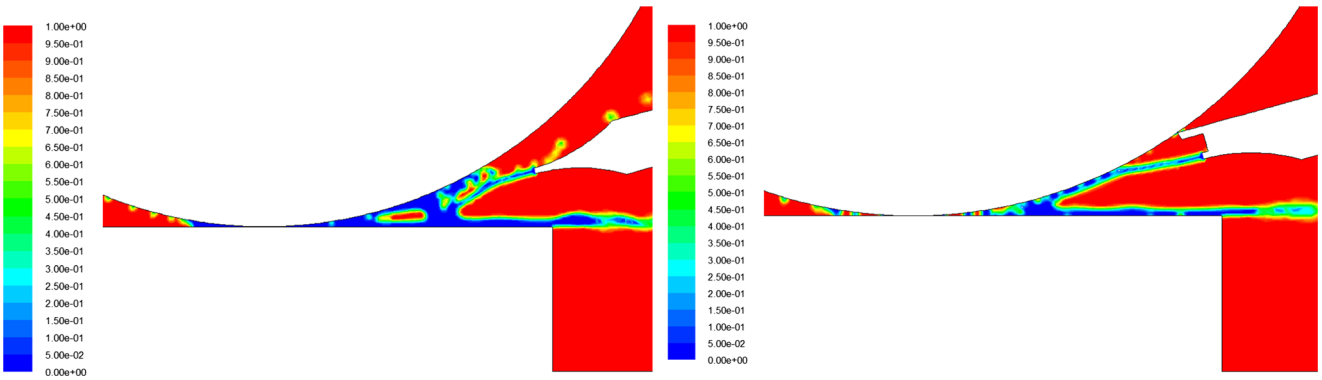

(a) No scraper (b) Scraper I

Fig. 8 Volume fraction distribution of airflow in grinding under conditions with and without scraper I (v_s=80 m/s): **a** no scraper and **b** scraper I

and the flow velocity is small near the bottom of the scraper. The increase of the distance from the scraper results in the increase of the gas barrier layer thickness and flow rate, which means that the gas barrier layer is rebuilt. The increase of the grinding wheel rotation speed results in the increase of the gas barrier layer thickness and flow velocity. Using the scraper weakens the effect of the gas barrier layer on the grinding wheel rotation, which can reduce the supply of grinding fluid barrier in the grinding process. However, the scraper is located below the scraper blade, and the gas barrier layer is regenerated. Thus, the scraper should be placed above the nozzle to minimize the effect of the gas barrier on the effective supply of the grinding fluid and to improve the flow rate.

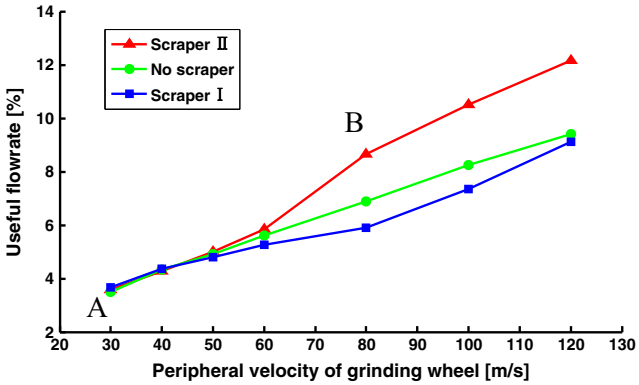

Fig. 10 Comparison of useful flow rate under different scraper conditions (v_j=20 m/s)

4.1 Optimal design and analysis of simulation results

We adopted air scraper and proper angle of the nozzle to improve the useful flow rate of the grinding fluid. In the proposed optimal scheme, the shape and position of the scraper are different, whereas other parameters in the flow field are the same. The simulation parameters are shown in Table 2.

4.1.1 Scheme A

Scheme A uses scraper I model, as shown in Fig. 6, with the scraper and the nozzle as a whole. The scraper is positioned above the nozzle; the vertical distance is 8 mm, and the distance between the front end and the wheel surface is 50 μm.

Figure 7 illustrates the comparison of the simulation results of the useful flow rate under conditions with and without the scraper, in which the grinding fluid jet velocity v_j is 20 m/s. The effect of using scraper I is not good, as shown in Fig. 7. The useful flow rate of the grinding fluid obtained from the simulation is less than that under conditions without the scraper. Given that the grinding liquid jet is at a constant velocity, the useful flow and useful flow rate are proportional to each other. Thus, the variation trend is the same. Figure 8 illustrates the fraction distribution volume of airflow field simulation under conditions with and without scraper I. The peripheral speed of the grinding wheel is 80 m/s. Figure 8a, which shows the condition with a scraper, and Fig. 8b, which shows the condition using scraper I, correspond to point A and point B in Fig. 7, respectively. Figure 8 illustrates that the grinding wheel is mixed with a certain amount of air at the entrance of the jet grinding area without the use of the scraper and is affected by the gas barrier layer caused by wheel rotation. On the contrary, when scraper I is used, the grinding wheel is affected by the air pressure difference, and the jet grinding fluid flows along the grinding wheel surface to the workpiece interface. Thus, the grinding fluid is mixed with a large amount of air. Figure 8 also illustrates that the airflow between the grinding wheel and the workpiece is more than the airflow under the condition without the scraper. The possible reason is that the space between the scraper and the nozzle is extremely large, and a formation of a certain gas barrier layer thickness at the surface of the grinding wheel occurs between the grinding fluid jet and the scraper, thereby reducing the useful flow rate of the grinding fluid. According to the preceding simulation analysis, the design of scraper I is not feasible and therefore cannot improve the useful flow rate of the grinding fluid. The design needs further optimization and enhancement.

Fig. 9 Scraper II model

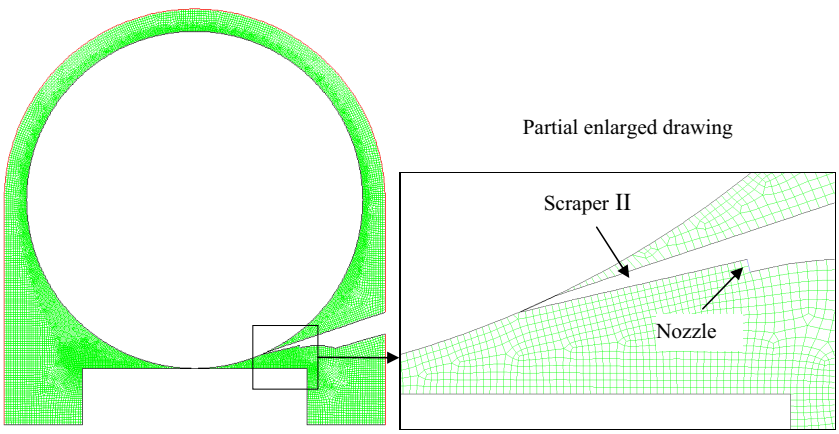

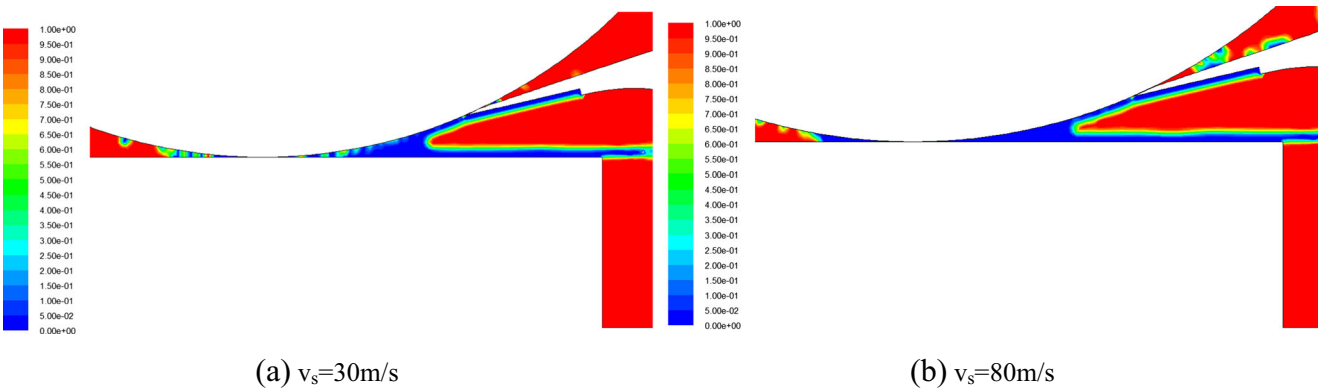

Fig. 11 Volume fraction distribution of airflow in grinding under the condition of using scraper II (v_j=20 m/s): **a** v_s=30 m/s and **b** v_s=80 m/s

4.1.2 Scheme B

According to scheme A analysis, a certain gas barrier layer thickness on the surface of the grinding wheel is formed between the grinding fluid jet and the scraper because the space between the scraper and the nozzle is considerably large. Thus, the useful flow rate of the grinding fluid is reduced. If the clearance between the scraper and the nozzle is reduced to 0, the effect of the gas barrier layer on the grinding liquid jet can be minimized. Considering the preceding analysis, we designed scheme B and used scraper II model, as shown in Fig. 9. The scraper is directly arranged above the nozzle outlet boundary. The minimum distance between the front end and the wheel surface is 50 μm. Thus, the grinding fluid is sprayed to the grinding zone along the scraper, which can further reduce the gas barrier layer on the effective supply of the grinding fluid.

Figure 10 illustrates the comparison of useful flow rates for the simulation of different scraper conditions in which the jet velocity of the grinding fluid is 20 m/s. The useful flow rates are obtained under the conditions with scraper II and scraper I as well as the condition without any scraper. When the wheel speed is less than 60 m/s, the grinding fluid flow rate obtained with scraper II is consistent with the simulation under the condition without using the scraper, as shown in Fig. 10. However, the effect of using scraper II is significantly improved, with useful flow rate increased significantly, when the peripheral speed of the grinding wheel is greater than 60 m/s. Scraper II model is improved based on scraper I. The comparison of the useful flow rate indicates the good effect of the improved model of the scraper. Under certain speed of the grinding wheel, the grinding fluid flow rate can be improved effectively with the scraper II model. Figure 11 illustrates the fraction distribution volume of airflow field simulation in grinding under the condition of using scraper II, in which the injection speed is 20 m/s. Figure 11a, which shows that the v_s wheel speed is 30 m/s, and Fig. 11b, which shows that the v_s wheel speed is 80 m/s, correspond to point A and point B in Fig. 10, respectively. The grinding fluid runs along the scraper and grinding wheel surface to the grinding zone through scraper II, as shown in Fig. 11. The scraper contributes to the weakening of the gas barrier layer. Although the distance between the front end of the scraper and the grinding wheel surface is relatively small (50 μm), the wheel rotation still carries a portion of the air through the gap into the jet grinding fluid. The air mixed into the grinding fluid is increased when the peripheral speed of the grinding wheel is 30 m/s, as shown in Fig. 11a. Point A in Fig. 10 illustrates that the grinding fluid flow rate slightly changes. The air mixed into the grinding fluid is relatively small when the

Fig. 12 Scraper III model

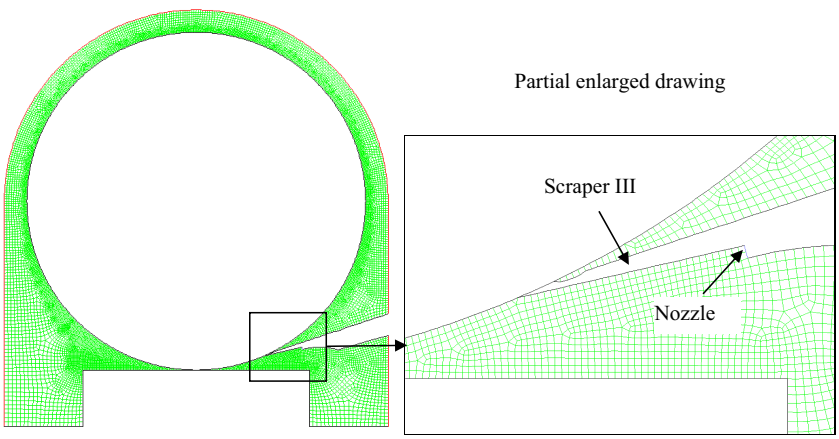

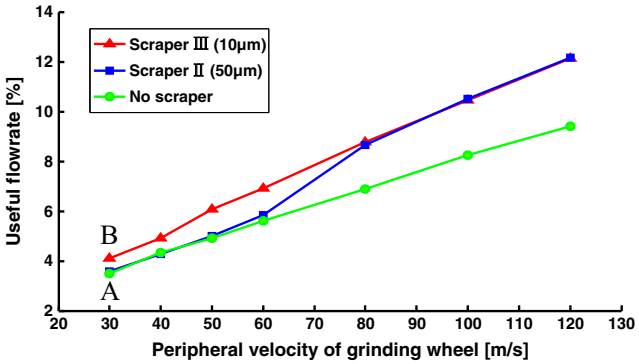

Fig. 13 Comparison of useful flow rate in different scraper conditions (v_j=20 m/s)

peripheral speed of the grinding wheel is 80 m/s, as shown in Fig. 11b. Point B in Fig. 10 illustrates that the grinding fluid flow rate is improved. According to the preceding analysis, scraper II, which is improved based on scraper I, can enhance the useful flow rate of the grinding fluid. However, some air infiltrations into the grinding fluid jet still occur, thereby affecting the effective supply of the grinding fluid. The useful flow rate does not increase when the wheel speed is low. Thus, further optimization and improvement of the original scheme is necessary.

4.1.3 Scheme C

The analysis of scheme B indicates that the grinding wheel still carries part of air through the gap of the scraper and the wheel surface into the jet grinding fluid, which affects the useful flow rate of the grinding fluid supply. If we narrow the distance between the scraper and the grinding wheel surface, we can further reduce the airflow in the grinding fluid to improve the useful flow rate. In view of the preceding analysis, scheme C narrows the distance down to 10 μm based on scheme B, which uses scraper III as shown in Fig. 12.

Figure 13 illustrates the useful flow rate comparison under different scraper conditions. The grinding fluid jet velocity v_j is 20 m/s. The three useful flow rates obtained through the simulation of conditions in which scrapers III and II are used as well as the condition without using the scraper are compared. As shown in Fig. 13, the effect of using scraper III is better than that of using scraper II. However, when the peripheral speed of the grinding wheel is greater than 80 m/s, the useful flow rates obtained by scrapers III and II are the same. The new model can improve the effective rate of the grinding fluid flow when the grinding wheel speed range is narrow. Thus, narrowing the distance between the scraper and the front wheel surface has a certain effect, which can further reduce the effect of the barrier layer on the effective supply of the grinding fluid. Figure 14 illustrates the fraction distribution volume of airflow field simulation in grinding under the condition of using different scrapers, in which the injection speed is 20 m/s and the peripheral speed of the grinding wheel is 30 m/s. Figure 14a, b corresponds to point A and point B in Fig. 13, respectively. Figure 14 illustrates that using scraper III reduces the distance between the scraper and the grinding wheel surface. Thus, the air mixed into the grinding fluid is

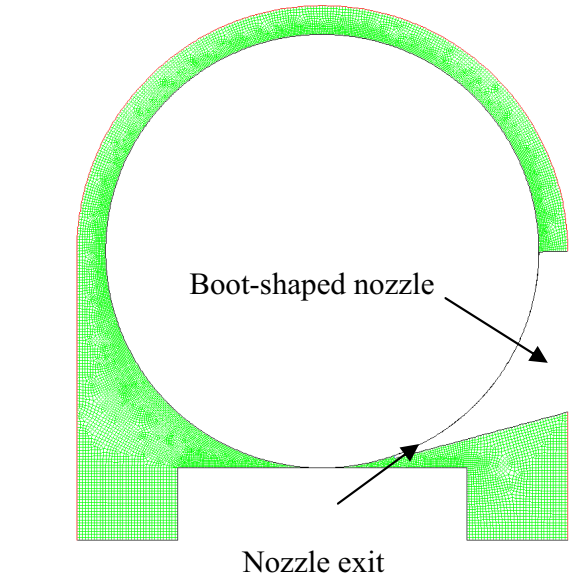

Fig. 15 Model of boot-shaped nozzle

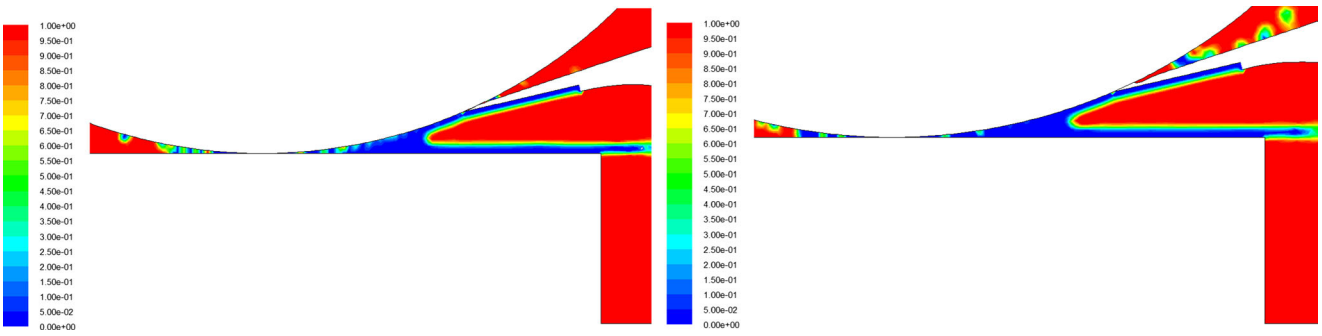

Fig. 14 Volume fraction distribution of airflow in grinding under the conditions in which different scrapers are used (v_s=30 m/s): **a** scraper II and **b** scraper III

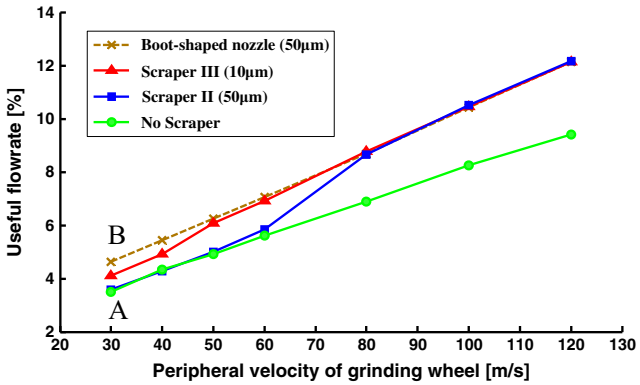

Fig. 16 Comparison of useful flow rate obtained through simulation with different scrapers (v_j=20 m/s)

reduced accordingly, which improves the grinding fluid flow rate. In general, the model optimization has achieved the anticipated effect to improve the useful flow rate.

4.1.4 Scheme D

Based on the preceding analysis, the effect of improved scheme C is good, which can improve the useful flow rate of the grinding fluid. With reference to the relevant literature, we increase the arc angle in front of the scraper and design scheme D to further reduce the influence of the gas barrier layer on the grinding fluid supply. This scheme uses the boot-shaped nozzle model, as shown in Fig. 15, with the arc angle at the front end of the nozzle of 70° and the distance between the grinding wheel surface of 50 μm. We expect that this scheme can further improve the useful flow rate of the grinding fluid. Figure 16 illustrates the useful flow rate comparison under the conditions of using different scrapers, where the grinding fluid jet velocity of v_j is 20 m/s. Figure 16 illustrates the comparison of the four useful flow rates of the conditions of using the boot-shaped nozzle scraper, scraper II, and scraper III as well as the flow rate under the condition without the scraper. Figure 16 also illustrates that using a boot-shaped nozzle is the best option. However, the useful flow rates of using the boot-shaped nozzle scraper, scraper III, and scraper II are the same when the peripheral speed of the grinding wheel is greater than 80 m/s. The maximum rate of useful flow is obtained with the boot-shaped nozzle when the peripheral speed of the grinding wheel is less than 80 m/s. Figure 17 illustrates the fractional distribution volume of the airflow field simulation in grinding with different scrapers, in which the speed of grinding wheel v_s is 30 m/s and the grinding fluid jet velocity is 20 m/s. Figure 17a, b illustrates the simulation results obtained with scraper II and boot-shaped nozzle, which correspond to point A and point B in Fig. 16. Although the distances between the two scrapers and the front end of the grinding wheel surface are all 50 μm, using the large arc angle boot-shaped nozzle leads to minimal air mixing into the jet grinding fluid. Thus, the useful flow rate of the grinding fluid is high. In the four schemes, the boot-shaped nozzle scheme is superior to the other schemes, thereby realizing the expected goal of improving the useful flow rate of the grinding fluid.

4.1.5 Scheme E

In scheme D, the distance between the boot-shaped nozzle and the grinding wheel surface is 50 μm. We narrow the distance to 10 μm in scheme E to further reduce the influence of the barrier layer on the grinding fluid jet.

Figure 18 illustrates the comparison of the useful flow rates under different conditions, of which the grinding fluid jet velocity v_j is 20 m/s. The useful flow rates of conditions of using schemes C, D, and E, and the flow rate of the condition without using the scraper are compared. In scheme E, the distance between the nozzle and the grinding wheel surface is narrowed to 10 μm, as shown in Fig. 18. However, the simulation result shows that the effect is not good. The useful flow rate of scheme E is lower than that of scheme D. The comparison of simulation results indicates that the air pressure between the boot-shaped nozzle and the grinding wheel surface is negative. At the distance of 10 μm, the minimum pressure range of the internal air is -2.94×10^5 (N/m^3) to -2.53×10^5 (N/m^3). At the spacing of 50 μm, the minimum pressure range

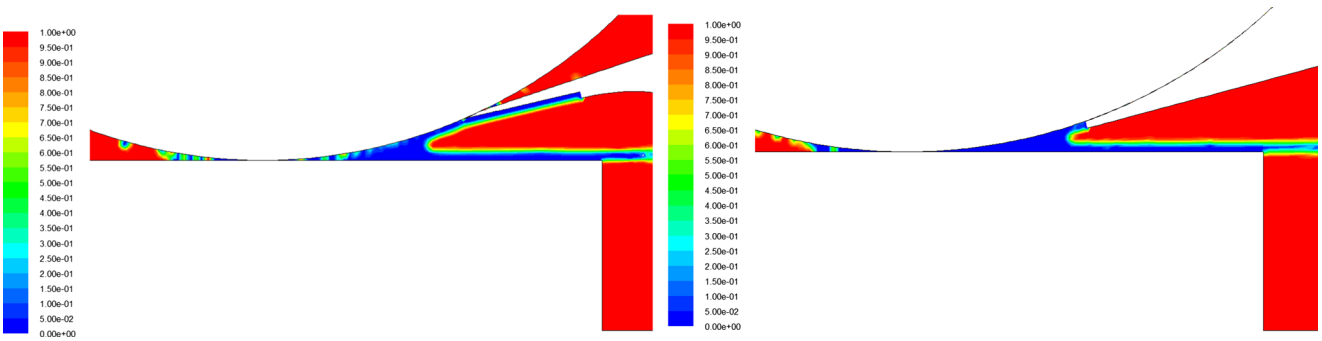

(a) Scraper II (b) Boot-shaped nozzle

Fig. 17 Contours of volume fraction of air in the grinding flow field obtained through simulation with different scrapers (v_s=30 m/s): **a** scraper II and **b** boot-shaped nozzle

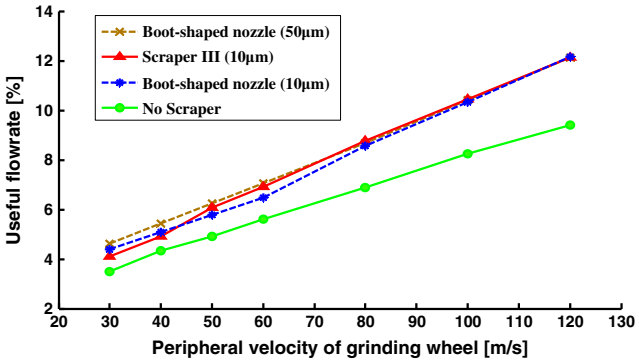

Fig. 18 Comparison of useful flow rate under different conditions

of the internal air is -8.97×10^4 (N/m^3) to -4.83×10^4 (N/m^3). The minimum pressure range of internal air when the distance is 10 μm is lower than that when the distance is 50 μm. When the distance is 10 μm, the airflow mixes into the grinding fluid, which also increases accordingly. Therefore, the useful flow rate is lower than that when the distance is 50 μm.

Figure 19 illustrates the useful flow rate changes of different grinding jet velocities through different forms of nozzles under the condition that the peripheral speed of the grinding wheel is 30 m/s. Along with the increase of grinding fluid jet velocity, the useful flow rate shows a downward trend, as illustrated in Fig. 19. This phenomenon occurs because the useful flow rate is the ratio of the useful grinding fluid flow and the jet flow. When the grinding wheel peripheral speed is determined, the useful flow and jet flow increase along with the increase of the grinding fluid jet velocity. However, the jet flow increase is significantly greater than the useful flow rate increase. Thus, the useful flow rate decreases. Figure 19 illustrates the comparison of the useful flow rates of schemes C, D, and E, and the condition without the scraper. As shown in Fig. 19, using schemes C, D, and E can improve the useful flow rate of the grinding fluid, which is consistent with the analysis results presented earlier in this paper. Scheme D has the best effect as it shows the highest flow rate. In scheme E, although the distance is reduced to 10 μm, the useful flow rate is slightly lower than that of scheme D.

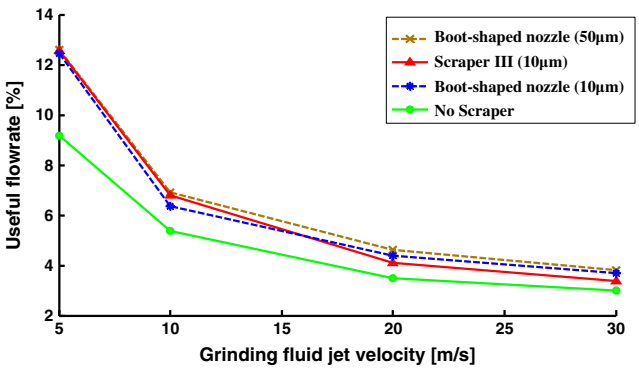

Fig. 19 Comparison of useful flow rate obtained with simulation under different conditions (v_s=30 m/s)

5 Conclusions

The improvement of the useful flow and flow rate of the grinding fluid has been investigated in previous studies via modeling, simulation, and experiment, and optimized grinding parameters were achieved [35, 49]. In this paper, a new method of *air scraper* was presented and simulated with focus on the air boundary layer and reflux around the grinding wheel.

In view of the influence of the barrier layer on the effective supply of the grinding fluid, using the scraper was proposed to destroy the gas barrier layer. The influence of the scraper on the gas barrier layer was analyzed through the simulation of the grinding gas flow field. Simulation was conducted at unified grinding parameters presented in this paper. Several schemes are designed to improve the fluid flow rate effectively. The simulation results of the gas/liquid flow and constant improvement were applied to these schemes. The results indicated the following:

The use of the scraper weakened the effect of grinding wheel rotation on the gas barrier layer, which can reduce the barrier on the supply of grinding fluid in the grinding process. However, because the gas barrier layer is regenerated under the scraper, it should be placed above the nozzle to minimize the effect of the gas barrier on the effective supply of the grinding fluid and to increase the fluid flow rate.

In the five schemes used to improve the fluid flow rate, the effect of schemes A and B is not ideal, whereas schemes C, D, and E achieve good results. The latter three schemes can improve the useful flow rate in the studied grinding parameter range, wherein scheme D is the best because it obtained the highest useful flow rate.

Regardless of the kind of scrapers used, the proper distance between the front end and the grinding wheel surface must be maintained. This distance must not be extremely large; otherwise, the weakening effect on the gas barrier layer is very limited. The distance must not be extremely small either. For example, in scheme E, the distance is narrowed to 10 μm based on scheme D. However, airflow within the gap increases because of increased internal air pressure. Thus, the air mixed into the grinding fluid also increased accordingly. Therefore, the useful flow rate of scheme E is lower than that of scheme D in which the distance is 50 μm.

Acknowledgments This research was financially supported by the National Natural Science Foundation of China (51175276), Qingdao Science and Technology Program of Basic Research Projects (14-2-4-18-jch), and Huangdao District Application Science and Technology Project (2014-1-55).

References

1. Nguyen TA, Butler DL (2005) Simulation of precision grinding process, part 1: generation of the grinding wheel surface. Int J Adv Manuf Technol 45(11):1321–1328

2. Hou YL, Li CH, Zhang DK, Jia DZ, Wang S (2014) Grinding temperature with nanoparticle jet minimum quantity lubrication. Recent Pat Mech Eng 7(2):149–161
3. Malkin S, Guo C (2007) Thermal analysis of grinding. CIRP Ann Manuf Technol 56(2):760–782
4. Brinksmeier E, Aurich JC, Govekar E (2006) Advances in modeling and simulation of grinding processes. CIRP Ann Manuf Technol 55(2):667–697
5. Ebbrell S, Woolley NH, Tridimas YD, Allanson DR, Rowe WB (2000) The effects of cutting fluid application methods on the grinding process. Int J Mach Tools Manuf 40(2):209–223
6. Mao C, Zou HF, Zhou X, Huang Y, Gan HY, Zhou ZX (2014) Analysis of suspension stability for nanofluid applied in minimum quantity lubricant grinding. Int J Adv Manuf Technol 71:2073–2081
7. Frank C, Wojciech Z, Edwin F (2004) Fluid performance study for groove grinding a nickel-based superalloy using electroplated cubic boron nitride (CBN) grinding wheels. J Manuf Sci Eng 126(3):451–458
8. Gao Y, Tse S, Mak H (2003) An active coolant cooling system for applications in surface grinding. Appl Therm Eng 23(5):523–537
9. Mao C, Zou HF, Huang Y, Li YF, Zhou ZX (2013) Analysis of heat transfer coefficient on workpiece surface during minimum quantity lubricant grinding. Int J Adv Manuf Technol 66:363–370
10. Morgan MN, Jackson AR, Wu H, Baines-Jones V, Batako A, Rowe WB (2008) Optimisation of fluid application in grinding. CIRP Ann Manuf Technol 57(1):363–366
11. Winter M, Li W, Kara S, Herrmann C (2014) Stepwise approach to reduce the costs and environmental impacts of grinding processes. Int J Adv Manuf Technol 71(5-8):919–931
12. Weinert K, Inasaki I, Sutherland JW (2004) Dry machining and minimum quantity lubrication. Ann CIRP 53(2):323–349
13. Park KH, Olortegui YJ, Yoon MC (2010) A study on droplets and their distribution for minimum quantity lubrication (MQL). Int J Mach Tools Manuf 50(9):824–833
14. Donaldson K, Li XY, MacNee W (1998) Ultrafine (nanometer) particle mediated lung injury. J Aerosol Sci 29(5):553–560
15. Kaliszer H, Trmal G (1975) Mechanics of grinding fluid delivery. SME Tech. Paper
16. Campbell JD (1993) An investigation of the grinding fluid film boiling limitation. Technical papers-Society of Manufacturing Engineers-all series
17. Campbell JD (1995) Optimized coolant application. Technical papers- Society of Manufacturing Engineers-all series
18. Ganesan M, Guo C, Malkin S (1995) Measurement of hydrodynamic forces in grinding. Transactions-North American Manufacturing Research Institution of SME 103–108
19. Ganesan M, Guo C, Ronen A (1996) Analysis of hydrodynamic forces in grinding. Transactions-North American Manufacturing Research Institution of SME 105–110
20. Chang CC, Wang SH, Szeri AZ (1996) On the mechanism of fluid transport across the grinding zone. J Mech Des 118(3):332–338
21. Klocke F, Baus A, Beck T (2000) Coolant induced forces in CBN high speed grinding with shoe nozzles. CIRP Ann Manuf Technol 49(1):241–244
22. Hryniewicz P, Szeri AZ, Jahanmir S (2001) Application of lubrication theory to fluid flow in grinding: part I-flow between smooth surfaces. J Tribol 123(1):94–100
23. Hryniewicz P, Szeri AZ, Jahanmir S (2001) Application of lubrication theory to fluid flow in grinding: part II—influence of wheel and workpiece roughness. J Tribol 123(1):101–107
24. Guo C, Malkin S (1992) Analysis of fluid flow through the grinding zone. J Eng Ind ASME 114(2):427–434
25. Engineer F, Guo C, Malkin S (1992) Experimental measurement of fluid flow through the grinding zone. J Eng Ind 114(4):61–66
26. Gviniashvili V, Webster J, Rowe B (2005) Fluid flow and pressure in the grinding wheel-workpiece interface. J Manuf Sci Eng 127(1): 198–205
27. Gviniashvili V, Rowe WB, Morgan MN (2004) Useful flowrate based on grinding power. J Key Eng Mater 257–258:333–338
28. Gviniashvili V, Woolley NH, Rowe WB (2004) Useful coolant flowrate in grinding. Int J Mach Tools Manuf 44(2):629–636
29. Gviniashvili V, Webster J, Rowe B (2005) Fluid flow and pressure in the grinding wheel-workpiece interface. Trans ASME 127(2):198–205
30. Li CH, Hou YL, Fang Z (2011) Analytical and experimental investigation of grinding fluid hydrodynamic pressure at wedge-shaped zone. Int J Abras Technol 4(2):140–155
31. Li CH, Hou YL, Xiu SH, Cai GQ (2008) Model and simulation of slurry velocity and hydrodynamic pressure in abrasive jet finishing with grinding wheel as restraint. Key Eng Mater 375–376:449–453
32. Li CH, Cai GQ, Xiu SC (2007) Hydrodynamic pressure modeling and verification of contact zone on abrasive jet finishing with grinding wheel as restraint. Acta Armamentarii 28(2):202–205
33. Han ZL, Li CH (2013) Theoretical modeling and simulation of airflow field near grinding wheel. Int J Control Autom 6(4):145–155
34. Li CH, Han ZL (2013) Modeling and simulation of the airflow field in wedge-shaped zone during the high-speed grinding. Int J Abras Technol 6(2):114–131
35. Li CH, Zhang XW, Zhang Q, Wang S, Zhang DK, Jia DZ, Zhang YB (2014) Modeling and simulation of useful fluid flow rate in grinding. Int J Adv Manuf Technol 75(9-12):1587–1604
36. Zheng JY, Li N, Jiang ZF (2009) Application study on two-phase flow field properties of grinding fluidic jet. Mach Tool Hydraul 37(1):20–23
37. Wang S, Li CH, Zhang DK, Jia DZ, Zhang YB (2014) Modeling the operation of a common grinding wheel with nanoparticle jet flow minimal quantity lubrication. Int J Adv Manuf Technol 74(5-8):835–850
38. Morgan MN, Barczak L, Batako A (2012) Temperatures in fine grinding with minimum quantity lubrication (MQL). Int J Adv Manuf Technol 60:951–958
39. Brinksmeier E, Minke E (1993) High-performance surface grinding—the influence of coolant on the abrasive process. Ann CIRP 42/1:367–370
40. Engineer F, Guo C, Malkin S (1992) Experimental measurement of fluid flow through the grinding zone. ASME J Eng Ind 114:61–66
41. Chang CC (1997) An application of lubrication theory to predict useful flow-rate of coolant on grinding porous media. Tribol Int 30(8):575–581
42. Jia DZ, Li CH, Zhang YB, Zhang DK, Zhang XW (2015) Experimental research on the influence of the jet parameters of minimum quantity lubrication on the lubricating property of Ni-based alloy grinding. Int J Adv Manuf Technol 1–14
43. Mao C, Tang XJ, Zou HF, Zhou ZX, Yin WW (2012) Experimental investigation of surface quality for minimum quantity oil–water lubrication grinding. Int J Adv Manuf Technol 59(1–4):93–100
44. Schumack MR, Chung J-B, Schultz WW (1991) Analysis of fluid flow under a grinding wheel. Trans ASME 113(5):190–197
45. Mandal B, Das GC, Das S, Banerjee S (2014) Improving grinding fluid delivery using pneumatic barrier and compound nozzle. Prod Eng 8(1-2):187–193
46. Mandal B, Singh R, Das S, Banerjee S (2011) Improving grinding performance by controlling air flow around a grinding wheel. Int J Mach Tools Manuf 51(9):670–676
47. Mandal B, Singh R, Das S, Banerjee S (2012) Development of a grinding fluid delivery technique and its performance evaluation. Mater Manuf Process 27(4):436–442
48. Heinemann R, Hinduja S, Barrow G, Petuelli G (2006) Effect of MQL on the tool life of small twist drills in deep-hole drilling. Int J Mach Tools Manuf 46:1–6
49. Li CH, Zhang Q, Zhang Q, Wang S, Zhang DK, Jia DK, Zhang YB, Zhang XW (2015) Useful fluid flow and flow rate in grinding: an experimental verification. Int J Adv Manuf Technol 1–10. doi:10.1007/s00170-015-7230-z